

A Ge/Si heterostructure nanowire-based double quantum dot with integrated charge sensor

YONGJIE HU^{1*}, HUGH O. H. CHURCHILL^{2*}, DAVID J. REILLY², JIE XIANG¹, CHARLES M. LIEBER^{1,3†}
AND CHARLES M. MARCUS^{2†}

¹Department of Chemistry and Chemical Biology, Harvard University, Cambridge, Massachusetts 02138, USA

²Department of Physics, Harvard University, Cambridge, Massachusetts 02138, USA

³School of Engineering and Applied Sciences, Harvard University, Cambridge, Massachusetts 02138, USA

*These authors contributed equally to this work.

†e-mail: cml@cmliris.harvard.edu; marcus@harvard.edu

Published online: 30 September 2007; doi:10.1038/nnano.2007.302

One proposal for a solid-state-based quantum bit (qubit) is to control coupled electron spins on adjacent semiconductor quantum dots^{1,2}. Most experiments have focused on quantum dots made from III–V semiconductors; however, the coherence of electron spins in these materials is limited by hyperfine interactions with nuclear spins^{3–6}. Ge/Si core/shell nanowires seem ideally suited to overcome this limitation, because the most abundant nuclei in Ge and Si have spin zero and the nanowires can be chemically synthesized defect-free with tunable properties⁷. Here, we present a double quantum dot based on Ge/Si nanowires in which we can completely control the coupling between the dots and to the leads. We also demonstrate that charge on the double dot can be detected by coupling it capacitively to an adjacent nanowire quantum dot. The double quantum dot and integrated charge sensor serve as an essential building block to form a solid-state qubit free of nuclear spin.

The potential of solid-state spin qubits is underscored by the recent demonstration of coherent spin control in gate-defined double quantum dots (DQDs) with integrated charge sensors in GaAs two-dimensional electron gases (2DEGs) (refs 3,4). Additionally, few-electron InAs nanowire single and double quantum dot devices possess strong spin-orbit interactions, which may prove useful for spin control^{8–10}. In III–V materials, however, hyperfine coupling limits electron spin coherence. As a result, the prospect of long coherence times in group IV materials due to the predominance of spin-zero nuclei¹¹ has stimulated several proposals^{12–15} and significant experimental effort. Experimental progress includes realizations of DQDs in carbon nanotubes^{16–18} and Si:P (ref. 19), as well as single dots in Si and Ge/Si nanowires^{7,20} and Si/Ge 2DEGs (refs 21–23).

The chemically synthesized Ge/Si core/shell heterostructure nanowires used here provide a high mobility one-dimensional hole gas with a mean free path on the order of hundreds of nanometres at room temperature⁷. The ~500 meV valence band offset between Ge and Si leads to a natural accumulation of holes in the Ge core, avoiding intentional impurity doping.

The DQD is formed by depleting a Ge/Si nanowire hole gas using metal gate electrodes. Three top gates, denoted L, M and R

in Fig. 1a, create barriers to define the dots, with the coupling between dots controlled by the middle barrier. Plunger gates LP and RP tune the energy levels of each dot. The device was measured in a dilution refrigerator with a base hole temperature, T_h , of 150 mK (see Methods).

Figure 1b–d shows the differential conductance of the DQD, g_{dd} , as a function of plunger voltages V_{LP} and V_{RP} . With the side barrier voltages fixed at $V_L = -0.55$ V and $V_R = 0$ V, changing the middle barrier voltage V_M shows three regimes of interdot coupling. For weak coupling ($V_M = -0.72$ V), transport occurs at triple points where the energy levels of the two dots align with the chemical potential of the leads, resulting in a rectangular array of high conductance points. Setting V_M to -0.85 V increases the coupling so that cross capacitance and tunnelling between dots split the triple points, creating the honeycomb charging pattern characteristic of DQDs (Fig. 1c) (ref. 24). For strong coupling ($V_M = -2.15$ V), a single dot is effectively formed (Fig. 1d). These data demonstrate fully tunable interdot coupling of the Ge/Si nanowire DQD.

Measuring the differential conductance of each single dot as a function of source-drain bias yields Coulomb diamonds (see Supplementary Information, Fig. S1), from which we extract charging energies $E_C = e^2/C_\Sigma$ of 3.1 (2.6) meV for the left (right) dot. Single-particle-level spacing ~ 250 μ eV was also measured from Coulomb diamonds. By counting the charge transitions before tunnel rates inhibit further measurement, we are able to place a lower bound of several hundred holes in each dot.

Key to realizing few-electron devices in 2DEGs is the ability to non-invasively read out the charge state of the DQD, even when the tunnel coupling to the leads makes the current immeasurably small²⁵. Among one-dimensional systems, charge sensing was demonstrated in a carbon nanotube single dot using a radio-frequency single-electron transistor²⁶. Here, we have developed a novel approach to charge sensing by capacitively coupling the DQD to a single dot on an adjacent nanowire. This method provides a simpler alternative in terms of fabrication. The charge sensor is a contact-defined dot capacitively coupled to the DQD with the coupler C (green, Fig. 1a). Gate S biases the sensor dot to the side of a Coulomb blockade peak for maximum sensitivity

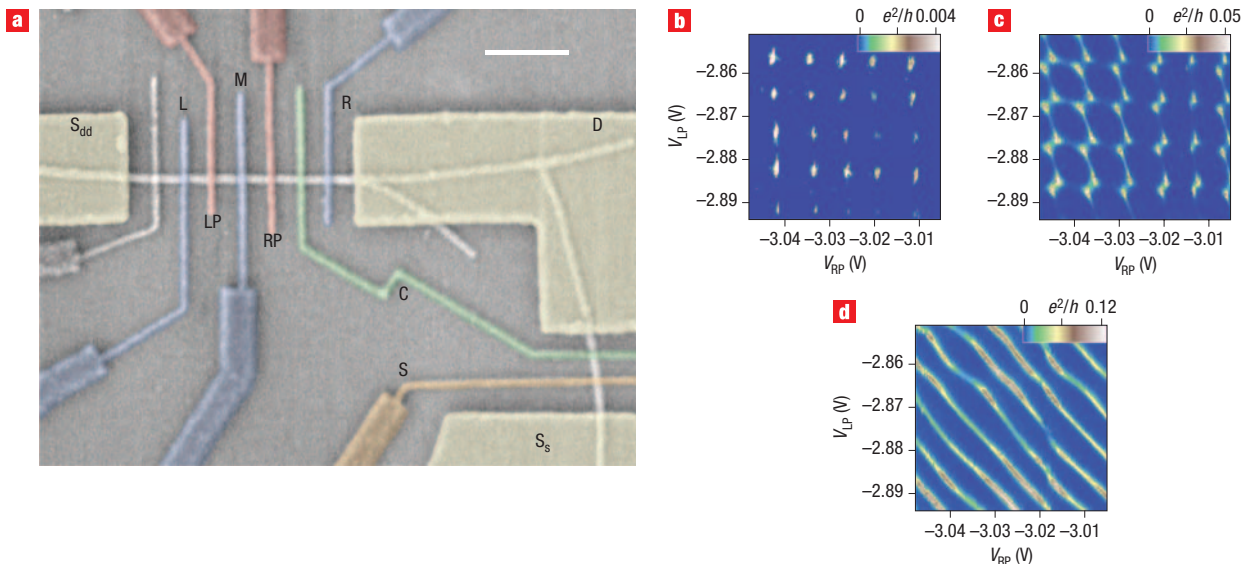


Figure 1 Ge/Si nanowire double dot device and demonstration of tunable interdot coupling. **a**, SEM image of the device used for all measurements. The double dot is formed with gates L, M and R, shown in blue, and the plunger gates LP and RP (red) tune the energy levels of each dot. On an adjacent nanowire, the charge sensor is a contact-defined single dot capacitively coupled to the double dot with the coupler C (green). The sensor is biased to the side of a Coulomb blockade peak using gate S (orange). The gate shown in grey was not used. S_{dd} , S_s and D label the double dot source, sensor source and shared drain contacts, respectively. Scale bar, 500 nm. **b–d**, Differential conductance (colour scale) is measured as a function of plunger voltages V_{LP} and V_{RP} . With the side barriers fixed at $V_L = -0.55$ V and $V_R = 0$ V, changing the middle barrier voltage V_M shows three regimes of interdot coupling. **b**, For weak interdot coupling ($V_M = -0.72$ V), transport is allowed on an array of triple points corresponding to resonant alignment of energy levels in the two dots with the chemical potential of the leads. **c**, At intermediate coupling ($V_M = -0.85$ V), cross-capacitance and tunnelling between dots split the triple points to create the honeycomb charging pattern. **d**, For strong coupling ($V_M = -2.15$ V), an effective single dot is formed, producing diagonal Coulomb blockade peaks.

to changes in the number of holes on the DQD (see Supplementary Information, Fig. S2).

To test the sensor, we made simultaneous transport and charge sensing measurements in the intermediate coupling regime ($V_M = -0.86$ V). Figure 2a shows the honeycomb pattern of g_{dd} as a function of V_{LP} and V_{RP} . Figure 2b shows the sensor conductance, g_s , measured simultaneously with g_{dd} and numerically differentiated with respect to V_{LP} . With the sensor biased on the negative slope of a Coulomb blockade peak, transfer of a hole from one dot to the leads produces a step up in conductance, whereas transfer of a hole from the left dot to the right dot results in a step down (see Supplementary Information, Fig. S2). These steps up and down are observed in Fig. 2b as bright and dark features, respectively.

To demonstrate the advantage of the sensor to probe regimes inaccessible to transport, we next decouple the DQD from the leads by setting $V_L = 0$ mV and $V_R = 250$ mV so that $g_{dd} < 10^{-5} e^2/h$. Figure 3a,b shows dg_s/dV_{LP} for both (a) strong and (b) weak interdot coupling. Clear honeycomb charging patterns are seen. In Fig. 3a the sensor dot is biased near the top of a Coulomb blockade peak, where g_s responds nonlinearly both to the charge transitions on the DQD and to the compensation (see Methods) applied to gate S, resulting in a peak in g_s rather than a step. We also note that the sign of dg_s/dV_{LP} in Fig. 3b is reversed relative to that in Fig. 2b because the sensor dot is biased in a positive slope position.

Significantly, the sensor also responds to interdot transitions at fixed total charge that are difficult to study in transport²⁷. Following the ‘detuning’ diagonal ϵ (dotted line, inset to Fig. 4)

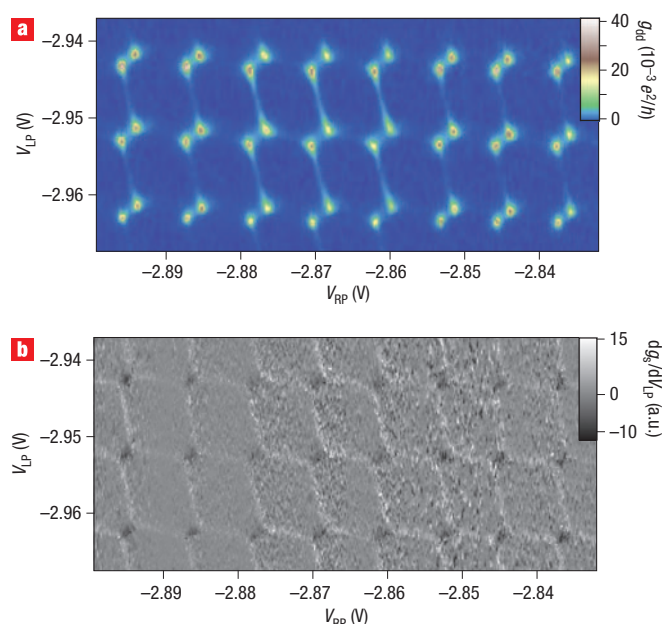


Figure 2 Simultaneous transport and charge sensing measurements. **a**, Double dot conductance g_{dd} as a function of gate voltages V_{LP} and V_{RP} . **b**, Simultaneously measured sensor dot conductance g_s , differentiated with respect to gate voltage V_{LP} .

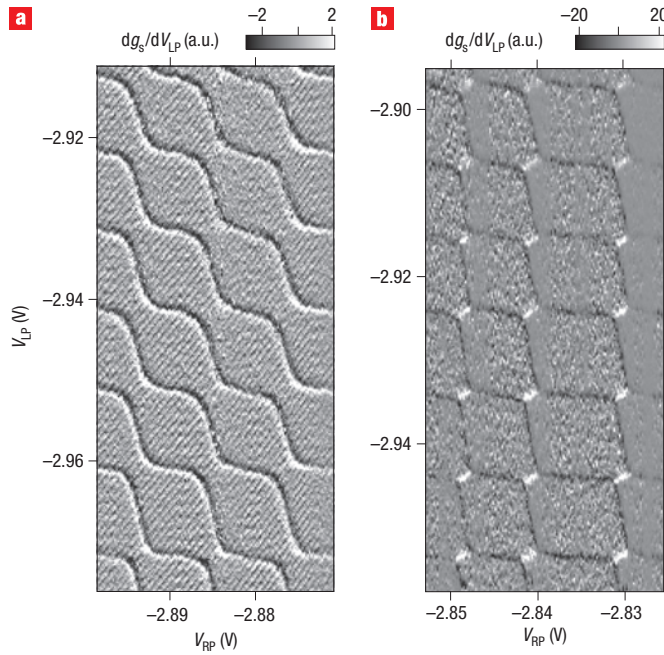


Figure 3 Charge sensing of an isolated double dot. Differentiated sensor conductance dg_s/dV_{LP} measured with the double dot weakly coupled to the leads ($g_{dd} < 10^{-5}e^2/h$) for strong ($V_M = -859$ mV; **a**) and weak ($V_M = -845$ mV; **b**) interdot coupling.

from negative to positive transfers charge from the right dot to the left dot, resulting in a sensor conductance step. Using (M, N) to denote the charge state with M (N) holes on the left (right) dot, we model the sensor conductance across the transition from $(M+1, N)$ to $(M, N+1)$ as an isolated two-level system in thermal equilibrium²⁷. When the tunnel coupling t is small relative to the individual dot single-particle level spacings, sensor conductance depends on detuning ϵ as

$$g_s = g_0 + \delta g \frac{\epsilon}{\Omega} \tanh\left(\frac{\Omega}{2k_B T_h}\right) \quad (1)$$

where $\Omega = \sqrt{\epsilon^2 + 4t^2}$ is the ground and excited state energy splitting. Rescaling the sensor conductance so that $g_0 = \delta g = 1/2$ yields the excess charge on the left dot, $\langle m \rangle - M$. Measurements of excess charge versus detuning are plotted in Fig. 4a,b, and good agreement is achieved by fits to the model of equation (1) (solid lines).

Because the transition width depends on both temperature and tunnelling, we first calibrate the hole temperature (which may be higher than thermometry readings) by measuring the transition at elevated temperatures where the holes are well thermalized (Fig. 4a). Data at the highest temperatures (0.75 and 1.0 K) provide the lever arm used to estimate a base hole temperature of 150 mK for the blue curve in Fig. 4a, in agreement with Coulomb blockade peak widths. We now examine the sensing transition as a function of interdot tunnelling in the regime $t \gtrsim k_B T_h$. Figure 4b shows excess charge along the detuning diagonal for several values of V_M at base temperature. For $V_M = -850$ mV the transition did not narrow for less negative V_M , indicating a thermally broadened transition with $t \sim 0$. For the more negative values of V_M , fixing $T_h = 150$ mK allows extraction of the tunnel couplings t as the only free parameter in fits to equation (1).

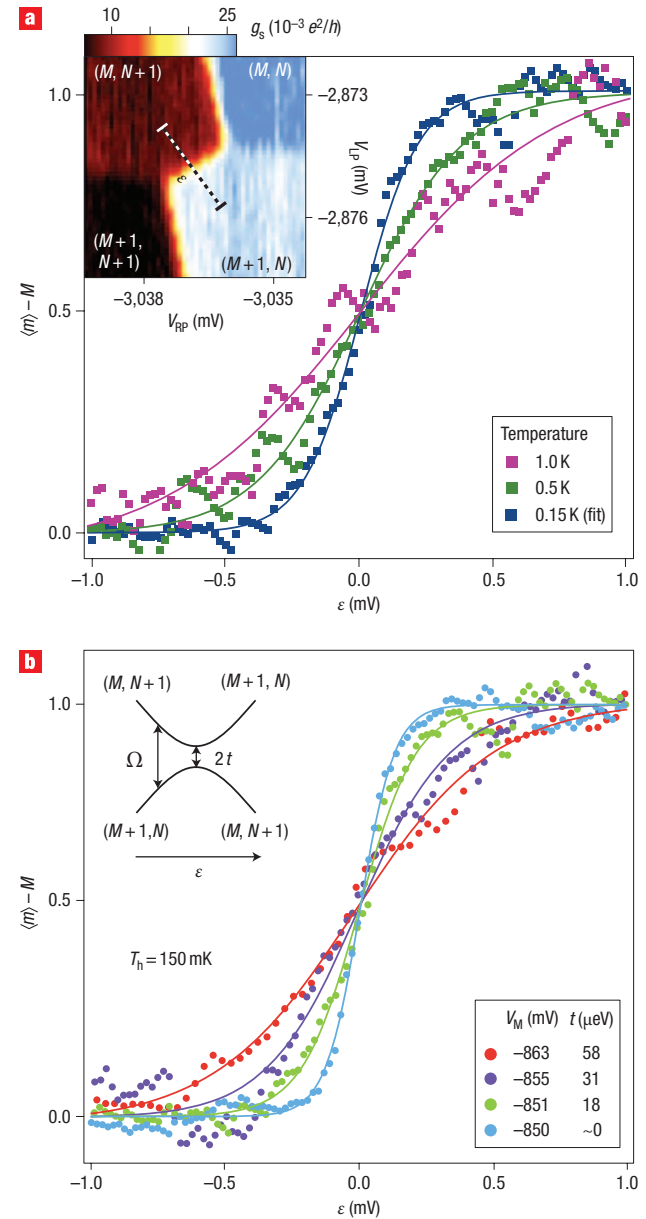


Figure 4 Interdot tunnelling measured with the charge sensor. **a**, Inset: sensor conductance g_s showing the charge stability diagram in the region used for **a** and **b**. The charge state with M (N) holes on the left (right) dot is denoted (M, N) . Average values of g_s are $6.5, 8.4, 23$ and $26 \times 10^{-3}e^2/h$ on the black, red, white and blue plateau, respectively. Main figure: sensor conductance g_s rescaled to reflect excess charge $\langle m \rangle - M$ (in units of e) on the left dot along the detuning diagonal ϵ (dotted line in inset shows $\epsilon = -1$ to 1 mV) at $T_h = 0.15$ K (dark blue), 0.5 K (dark green) and 1.0 K (pink) for $V_M = -851$ mV. The solid lines are fits to equation (1).

b, Excess charge on the left dot at base temperature for several values of V_M . The temperature-broadened curve (blue) widens as V_M is made more negative, increasing the tunnel coupling t , which is extracted from fits to equation (1) (solid lines). The fit to the temperature-broadened curve gives a base hole temperature of 150 mK, in agreement with Coulomb blockade peak widths. Inset: schematic energy diagram of the two-level system model, showing the splitting between ground and excited states as a function of detuning ϵ with an anticrossing of $2t$ at $\epsilon = 0$. Each of the curves in **a** and **b** is an average of 100 sweeps, and the inset to **a** is an average of 35 two-dimensional scans.

In conclusion, we have demonstrated a fully tunable DQD in a Ge/Si heterostructure nanowire using local gate electrodes. We also present a novel approach to charge sensing by capacitively coupling the DQD to a single dot on an adjacent nanowire. Having integrated these two components, future devices may address the challenge of accessing the few-charge regime and carrying out coherent spin manipulation experiments. The prospects of forming spin qubits with Ge/Si nanowire DQDs are bright. Long spin coherence times are expected to result from suppressed hyperfine interactions due to the absence of nuclear spin. Because of strong spin-orbit interactions in the valence band, hole spin lifetimes are generally shorter than those of electrons, but appropriate conditions enhance hole spin lifetimes^{28,29}. In our system quantum confinement and strain-induced splitting of the heavy-hole and light-hole subbands may reduce spin-orbit interactions^{11,30}. Furthermore, the observed ambipolar behaviour in these nanowires⁷ ensures electron and hole conduction and suggests the possibility of studying electron and hole spins in the same device. This clean, highly controllable system offers a promising route to studies of coherent electronic devices free of nuclear spin.

METHODS

FABRICATION OF Ge/Si NANOWIRE DEVICES

The undoped Ge/Si core/shell nanowires were grown using a two-step chemical vapour deposition process⁷. The nanowires have an average core diameter of 14.6 nm and Si shell thickness of 1.7 nm, and normally exhibit ⟨110⟩ growth direction. Atomic force microscopy measurements of the nanowires forming the device presented here indicate ~15 nm diameter for the DQD nanowire and ~10 nm diameter for the sensor nanowire. The degenerately doped Si substrate with 600 nm thermal oxide served as a global backgate and was set to -2 V for all measurements. All source-drain contact electrodes (50 nm Ni) were defined by electron-beam lithography and deposited by thermal evaporation. Transparent contacts were obtained for the DQD nanowire, but contact barriers for the sensor nanowire formed a dot at low temperature, possibly due to its smaller diameter or to a thicker native oxide layer on the shell. The nanowires and source-drain electrodes were then covered with a 12 nm HfO₂ high dielectric constant layer ($\kappa \sim 23$) using atomic layer deposition. HfO₂ was deposited at 110 °C in 100 cycles of 1 s water vapour pulse, 5 s N₂ purge, 3 s precursor and 5 s N₂ purge. Tetrakis (dimethylamino) hafnium [Hf(N(CH₃)₂)₄] was used as precursor. Electron-beam lithography was used to define the top gates, followed by thermal evaporation of Al (50 nm). The top gates were approximately 30 nm wide with 110 nm spacing.

MEASUREMENTS

An a.c. excitation of 10 µV was applied to the source contacts of the DQD and sensor at 149 and 109 Hz, respectively. The shared drain contact was connected to a current preamplifier, followed by separate lock-in amplifiers to measure the DQD conductance g_{dd} and the sensor conductance g_s . To cancel the cross-coupling between gates and maintain the sensor in a high-sensitivity position, the sensor plunger voltage V_s was adjusted during sweeps of V_{LP} and V_{RP} .

Received 18 June 2007; accepted 29 August 2007; published 30 September 2007.

References

- Loss, D. & DiVincenzo, D. P. Quantum computation with quantum dots. *Phys. Rev. A* **57**, 120–126 (1998).
- Hanson, R., Kouwenhoven, L. P., Petta, J. R., Tarucha, S. & Vandersypen, L. M. K. Spins in few-electron quantum dots. *cond-mat/0610433* (2006).
- Petta, J. R. *et al.* Coherent manipulation of coupled electron spins in semiconductor quantum dots. *Science* **309**, 2180–2184 (2005).
- Koppens, F. H. L. *et al.* Driven coherent oscillations of a single electron spin in a quantum dot. *Nature* **442**, 766–771 (2006).
- Burkard, G., Loss, D. & DiVincenzo, D. P. Coupled quantum dots as quantum gates. *Phys. Rev. B* **59**, 2070–2078 (1999).
- Khaetskii, A. V., Loss, D. & Glazman, L. Electron spin decoherence in quantum dots due to interaction with nuclei. *Phys. Rev. Lett.* **88**, 186802 (2002).
- Lu, W., Xiang, J., Timko, B. P., Wu, Y. & Lieber, C. M. One-dimensional hole gas in germanium/silicon nanowire heterostructures. *Proc. Natl Acad. Sci. USA* **102**, 10046–10051 (2005).
- Fasth, C., Fuhrer, A., Björk, M. T. & Samuelson, L. Tunable double quantum dots in InAs nanowires defined by local gate electrodes. *Nano Lett.* **5**, 1487–1490 (2005).
- Fasth, C., Fuhrer, A., Samuelson, L., Golovach, V. N. & Loss, D. Direct measurement of the spin-orbit interaction in a two-electron InAs nanowire quantum dot. *Phys. Rev. Lett.* **98**, 266801 (2007).
- Pfund, A., Shorubalko, I., Ensslin, K. & Leturcq, R. Suppression of spin relaxation in an InAs nanowire double quantum dot. *cond-mat/0701054* (2007).
- Tyryshkin, A. M. *et al.* Electron spin coherence in Si. *Physica E* **35**, 257–267 (2006).
- Kane, B. E. A silicon-based nuclear spin quantum computer. *Nature* **393**, 133–137 (1998).
- Vrijen, R. *et al.* Electron-spin-resonance transistors for quantum computing in silicon–germanium heterostructures. *Phys. Rev. A* **62**, 012306 (2000).
- Friesen, M. *et al.* Practical design and simulation of silicon-based quantum-dot qubits. *Phys. Rev. B* **67**, 121301(R) (2003).
- Trauzettel, B., Bulaev, D. V., Loss, D. & Burkard, G. Spin qubits in graphene quantum dots. *Nature Phys.* **3**, 192–196 (2007).
- Biercuk, M. J., Garaj, S., Mason, N., Chow, J. M. & Marcus, C. M. Gate-defined quantum dots on carbon nanotubes. *Nano Lett.* **5**, 1267–1271 (2005).
- Sapmaz, S., Meyer, C., Beliczyński, P., Jarillo-Herrero, P. & Kouwenhoven, L. P. Excited state spectroscopy in carbon nanotube double quantum dots. *Nano Lett.* **6**, 1350–1355 (2006).
- Gräber, M. R. *et al.* Molecular states in carbon nanotube double quantum dots. *Phys. Rev. B* **74**, 075427 (2006).
- Chan, V. C. *et al.* Ion implanted Si:P double dot with gate tunable interdot coupling. *J. Appl. Phys.* **100**, 106104 (2006).
- Zhong, Z., Fang, Y., Lu, W. & Lieber, C. M. Coherent single charge transport in molecular-scale silicon nanowires. *Nano Lett.* **5**, 1143–1146 (2005).
- Klein, L. J., Savage, D. E. & Eriksson, M. A. Coulomb blockade and Kondo effect in a few-electron silicon–germanium quantum dot. *Appl. Phys. Lett.* **90**, 033103 (2007).
- Berer, T. *et al.* Lateral quantum dots in Si/SiGe realized by a Schottky split-gate technique. *Appl. Phys. Lett.* **88**, 162112 (2006).
- Sakr, M. R., Jiang, H. W., Yablonovitch, E. & Croke, E. T. Fabrication and characterization of electrostatic Si/SiGe quantum dots with an integrated read-out channel. *Appl. Phys. Lett.* **87**, 223104 (2005).
- van der Wiel, W. G., De Franceschi, S., Elzerman, J. M., Fujisawa, T., Tarucha, S. & Kouwenhoven, L. P. Electron transport through double quantum dots. *Rev. Mod. Phys.* **75**, 1–22 (2003).
- Elzerman, J. M. *et al.* Few-electron quantum dot circuit with integrated charge read out. *Phys. Rev. B* **67**, 161308(R) (2003).
- Biercuk, M. J. *et al.* Charge sensing in carbon-nanotube quantum dots on microsecond timescales. *Phys. Rev. B* **73**, 201402(R) (2006).
- DiCarlo, L. *et al.* Differential charge sensing and charge delocalization in a tunable double quantum dot. *Phys. Rev. Lett.* **92**, 226801 (2004).
- Bulaev, D. V. & Loss, D. Spin relaxation and decoherence of holes in quantum dots. *Phys. Rev. Lett.* **95**, 076805 (2005).
- Heiss, D. *et al.* Observation of extremely slow spin relaxation in self-assembled quantum dots. *cond-mat/0705.1466* (2007).
- Schäffler, F. High-mobility Si and Ge structures. *Semicond. Sci. Technol.* **12**, 1515–1549 (1997).

Acknowledgements

We thank L. DiCarlo and E. A. Laird for experimental assistance and helpful discussions. C.M.L. acknowledges support from the Defense Advanced Research Projects Agency and Samsung Electronics. C.M.M. acknowledges support from the Disruptive Technology Office. H.O.H.C. acknowledges support from the National Science Foundation.

Correspondence and requests for materials should be addressed to C.M.L. or C.M.M. Supplementary information accompanies this paper on www.nature.com/naturenanotechnology/.

Author contributions

Y.H. and H.O.H.C. performed the experiments. Y.H. and J.X. fabricated the devices. Y.H., H.O.H.C., D.J.R., C.M.L. and C.M.M. analysed the data and co-wrote the paper. All authors discussed the results and commented on the manuscript.

Reprints and permission information is available online at <http://npg.nature.com/reprintsandpermissions/>